Progress in Additive Manufacturing
https://doi.org/10.1007/s40964-024-00837-0

FULL RESEARCH ARTICLE

A comparative study on microstructure and mechanical properties of 17-4PH processed by a laser powder bed fusion vs rolling process

Thabet A. M. Sghaier[1] · Habib Sahlaoui[1] · Tarek Mabrouki[2] · Haifa Sallem[3] · Joël Rech[4]

Received: 15 April 2024 / Accepted: 7 October 2024

Abstract

This study provides a comprehensive benchmark comparison of microstructure, mechanical properties, and their evolution during subsequent heat treatment of 17-4PH Martensitic stainless steel (MSS) processed by laser powder bed fusion (LPBF) and its commercially rolled counterparts. The results reveal that LPBF samples exhibit a finer martensitic microstructure with presence of structural defects, pores, and some non-metallic inclusions randomly distributed at the grain boundaries and within the grains and an almost absence of austenite, compared to rolled samples. Additionally, after identical heat treatment, LPBF samples maintain a relatively unchanged microstructure while aging of rolled samples leads to a reduction in martensite in favor of austenite and Cu- and Si-rich precipitates. The LPBF samples demonstrate slightly elevated hardness ($HV_{0.5}+20\%$), mechanical strength (UTS + 15%) compared to rolled ones. Nevertheless, LPBF samples display a distinct behavior, characterized by abrupt fracture and reduced elongation at failure (El% max. 4% vs. 17.5%). Specifically, failure in LPBF samples is attributed to cleavage and cavities' coalescence contrasting with the progressive failure mechanism observed in rolling ones driven by plasticity and damage evolution. Furthermore, the impact resistance of LPBF samples is notably weak (K max. 12.5 J/cm^2 vs. 155 J/cm^2), which is likely caused by macro- and microstructural defects generated by the LPBF process and the nucleation of harmful precipitates. The study proposes that the ductility of LPBF samples could be improved by implementing appropriate heat treatment and reducing defects through parameter optimization and by specific thermal cycle control during the LPBF process.

Keywords 17-4PH martensitic stainless steel · Laser powder bed fusion · Rolling · Microstructure · Mechanical properties · Heat treatment

✉ Haifa Sallem
haifa.sallem@hes-so.ch

Thabet A. M. Sghaier
thabetsgaier@gmail.com

Habib Sahlaoui
habib.sahlaoui@ensit.rnu.tn

Tarek Mabrouki
tarek.mabrouki@enit.utm.tn

Joël Rech
Joel.rech@enise.fr

[1] Laboratory of Mechanics, Materials and Processes (LMMP) LR 99ES05, University of Tunis (UT), National High School of Engineering of Tunis (ENSIT), 5 Avenue Taha Hussien, 1008, B.P 56, Bab Menara, Tunis, Tunisia

[2] Applied Mechanics and Engineering Laboratory (LMAI-LR-11ES19), University of Tunis El Manar, National Engineering School of Tunis (ENIT), BP-37, Le Belvedere 1002, Tunis, Tunisia

[3] Institute of Systems Engineering, HEI of HES-SO Valais-Wallis, HES-SO University of Applied Sciences and Arts Western Switzerland, Rue de l'Industrie 23, 1950 Sion, Switzerland

[4] Laboratoire de Tribologie et Dynamique des Système (LTDS-UMR5513), ECL-ENISE, 58, rue Jean Parot, 42023 Saint-Etienne cedex 2, France

Published online: 24 October 2024

1 Introduction

The 17-4PH is a hardening martensitic stainless steel (MSS) that offers, besides its high corrosion resistance, attractive mechanical properties which can be adapted, according to the conditions of use, by simple heat treatments. Basing on the most of its versatile potential, the 17-4PH MSS is extensively used in various sectors (chemical, petrochemical, food, offshore, aerospace, automotive, etc.) and for several applications (valves and engine components, turbine blades, gears, shafts, aircraft structures, surgical and dental instruments, etc.).

During this last decade, there has been growing interest in 17-4PH MSS by industrialists due to its remarkable suitability for new additive manufacturing (AM) techniques. This has generated enthusiasm among various scientific communities in different disciplines. The emergence and development of new AM techniques and processes have made it possible to manufacture parts and structures from materials that were previously challenging to cast or mold. Furthermore, AM provides greater flexibility and numerous advantages compared to conventional manufacturing methods and processes. It enables the production of highly intricate geometries with exceptional precision while reducing costs, time, and material waste. It is a significant improvement over traditional manufacturing processes. Therefore, many researchers dedicate their work to develop new AM process and improving the quality of products obtained by AM, focusing on improving some aspects such as morphology, surface roughness, mechanical and physicochemical properties, reliability, accessibility, etc.

Bertocco et al. [4] and Leo et al. [17] considered that the laser powder bed fusion (LPBF) process, also known as selective laser melting (SLM), is suitable for AM of components and structures from 316 and 17-4PH SS. In particular, Bertocco et al. [4] have underlined the relevance of LPBF for the fabrication of lattice structures, highlighting the quality of geometric precision and structural consistency of the lattice, as well as the satisfactory behavior of these structures. Nevertheless, AM by LPBF greatly influences the resulting microstructure and can leads to undesirable effects on the mechanical and physicochemical properties influencing the in-service behavior of LPBF 17-4PH SS components and structures [16, 17, 31]. Specifically, residual stresses [2, 20, 21], anisotropy [8, 15], and porosities [5, 27], inclusions and oxides [11, 38] are the primary detrimental outputs of 17-4PH SS manufactured by the LPBF process.

Several studies have analyzed the quality of LPBF components and optimized manufacturing parameters [2, 15, 27]. Lee et al. [16] conducted a study on the effects of process parameters on the high-temperature behavior of 17-4PH to enhance mechanical resistance. They found that the microstructure, mechanical, and physicochemical properties of LPBF 17-4PH SS are distinctly different from those achieved through conventional manufacturing processes. An energy density level of 64.29 J/mm^3 and a scan speed exceeding 1884 mm/s were recommended to obtain 17-4PH LPBF parts with a compromise between material strength and minimal metallurgical defects.

As previously stated, the 17-4PH SS possesses a fully martensitic structure, characterized by a high yield strength, mechanical resistance, and hardness, but lower ductility compared to ferritic and austenitic steels. However, the 17-4PH SS and similar martensitic grades with structural hardening by precipitation are often subjected to aging treatments before use. The temperature and duration of the treatment are chosen according to the required mechanical properties. Indeed, the fine precipitation which occurs within the martensitic matrix during aging makes it possible to improve the ductility by reducing the internal stresses while preserving the high mechanical resistance of these materials [10, 13]. Choo et al. [7] and Merlin et al. [22] investigated the effect of heat treatment on the microstructure of 17-4PHSS manufactured by AM, aiming to enhance its hardness. It was found that the microstructure resulting from aging heat treatment contains a higher fraction of martensite compared to that resulting from solution annealing followed by aging, which provides a microstructure with significant fractions of austenite and δ-ferrite. Therefore, the aging heat treatment alone is adequate to provide considerable hardness to 17-4PH MSS eliminating the requirement for solution annealing.

In their study, Garcia et al. [11] compared the effects of solution treatment and aging process on the strength and biocompatibility of LPBF and rolled 17-4PH steel for biomedical applications. They concluded that post-processing heat treatment played a crucial role in developing a uniform microstructure and achieving hardness values equivalent to or superior to those observed in rolled 17-4PH. This improvement was attributed to the predominance of the martensitic structure and precipitation hardening in the solution-treated and aged steel, accompanied by an enhancement in corrosion resistance. Zhao et al. [38] reported that the solution annealing followed by aging heat treatment of LPBF 17-4PH had the ability to refine the martensitic microstructure and to enhance mechanical properties. They observed that after heat treatment, the martensite was refined, the yield strength and the elastic modulus of the porous 17-4PH stainless steel increased by 21% and 35%, respectively. Moreover, they noticed that the formation of precipitates such as M_7C_3, ε-Cu, NbC, and silica oxide SiO_2, leading to the degradation of the corrosion resistance.

It is widely agreed that microstructure, mechanical and physicochemical properties, and heat treatment responses are strongly linked to the LPBF process parameters (laser power, scanning speed, hatch spacing, layer thickness, etc.). Some researchers have added other factors such as the size and geometry of the manufactured part or structure, its relative orientation to the building direction, etc. Therefore, it is important to mention that each combination of LPBF working parameters leads to parts and structures with specific microstructure, mechanical properties and responses to thermal treatments. Consequently, the differences in microstructure and mechanical properties between LPBF and Rolled 17-4PH MSS remain unclear. Therefore, it is somewhat difficult, at the current state, to evaluate the capability of the LPBF process to replace the traditional method of 17-4PH MSS manufacturing. It is also difficult to judge on the reliability of components and structures produced by the LPBF process when used in potential applications and under severe conditions (high temperatures, aggressive environments, impacts, etc.).

As the 17-4PH is used in various and cutting-edge industries (aviation, automotive, medical, marine, nuclear, military, tooling, and petroleum sectors, etc.), the mechanical properties of such structures need to be thoroughly checked and investigated before putting these materials to practical applications. Consequently, the main objective of the present work is to highlight whether:

- The 17-4PH parts and structures manufactured by LPBF and those obtained by conventional techniques can have the same mechanical responses during service.
- The conventional normalizing thermal treatment, often used to optimize the mechanical properties of rolled or forged 17-4PH, can bring the same effects or not (regarding microstructure, mechanical properties; etc.) to those obtained by LPBF.

As such, a comparison study of the microstructure, microhardness, tensile strength, ductility, and impact resistance of the LPBF and rolled parts at the received state and after heat treatment was carried out. Accordingly, potential improvements in ductility and impact resistance of 17-4PH parts and structures additively manufactured by LPBF are required before putting them into operation. Appropriate heat treatment, parameter optimization, and specific thermal cycle control are likely necessary during and after the LPBF process.

2 Materials and methods

2.1 Materials

17-4PH MSS cylindrical bars with a diameter of 40 mm and a length of 5 m were commercially available under mill-annealed condition (known as condition A). The chemical compositions of the acquired 17-4PH, determined using EDS, are presented in Table 1.

The 17-4PH MSS virgin powder used to fabricate specimens by LPBF process is commercialized by Sandvik Osprey under the reference X5CrNiCuNb16-4. This powder exhibits a particle size distribution ranging between 15 and 45 µm. The average chemical composition is presented in Table 1.

2.2 Additive manufacturing of 17-4PH SS by LPBF process

A PROX200-Phenix machine was used to fabricate specimens of 17-4PH MSS by LPBF. It is equipped with a fiber-optic laser with a beam diameter of d = 70 µm, a maximum power of 300 W, and a scraper coated with tungsten carbide. The specimens are fabricated in a chamber with dimensions of $140 \times 140 \times 125$ mm^3 and on a 304L stainless steel plate preheated at 100 °C to reduce the effect of thermal stresses on fabricated samples. Nitrogen gas was used to inert the build chamber to prevent powder spillage, oxidation of the parts, and the formation of porosities during the LPBF process.

The LPBF parameters employed in the fabrication of the specimens are summarized in Table 2. These parameters correspond to an energy density E of 64 J$^{/mm3.}$

All specimens were fabricated using a hexagonal scanning strategy with 10 mm line spacing (Fig. 1), resulting in parallel lines that form hatching patterns due to the laser's back-and-forth movement over the fusion area. Between each fused layer, a 90° rotation was applied to mitigate texture effects (odd-numbered layers at 0°, even-numbered layers at 90°) with a 100 µm hexagon overlap to enhance surface quality, minimize residual stresses generated during fusion-solidification cycles, and ensure proper fusion between each pattern (Fig. 1). There was a 30% overlap between fusion lines to ensure complete fusion of the powder layer. The Z-axis of the specimen corresponds to the layer stacking direction (build direction).

A build plate containing 18 cylindrical specimens (Ø12 × 65 mm2) and 18 prismatic specimens

Table 1 Nominal composition (wt. %) of 17-4PH MSS used in this study, Fe balance

17-4PH	C	Si	Mn	Ni	Cr	Cu	Co	Nb + Ta	S	*P*
Rolled	< 0.07	0.4	0.78	4.46	16.53	4.2	0.03	0.42	0.02	0.01
Powder	< 0.07	< 1	< 1	3–5	15–17.5	3–5	0.03	0.15–0.45	< 0.03	< 0.04

$12 \times 12 \times 57$ mm3 intended for mechanical and microstructural characterization was digitally designed through computer-aided design (CAD) system and then additively manufactured using the previously mentioned parameters and strategy LPBF process (Fig. 2). The cylindrical and prismatic bars were oriented vertically to ensure tensile test specimen's geometry, to minimize residual stresses and to prevent defaults such as delamination, deformation, and cracking during the manufacturing process.

Table 2 Additive manufacturing parameters via LPBF

Laser power P (W)	Scan speed V (mm/s)	Jump speed (mm/s)	Hatch spacing h (µm)	Layer thickness e (µm)	Laser defocusing	Fused line overlap
240	2500	5000	50	30	0	30%

Energy density: $E = \frac{P}{V.h.e} = 64 J.mm^{-3}$

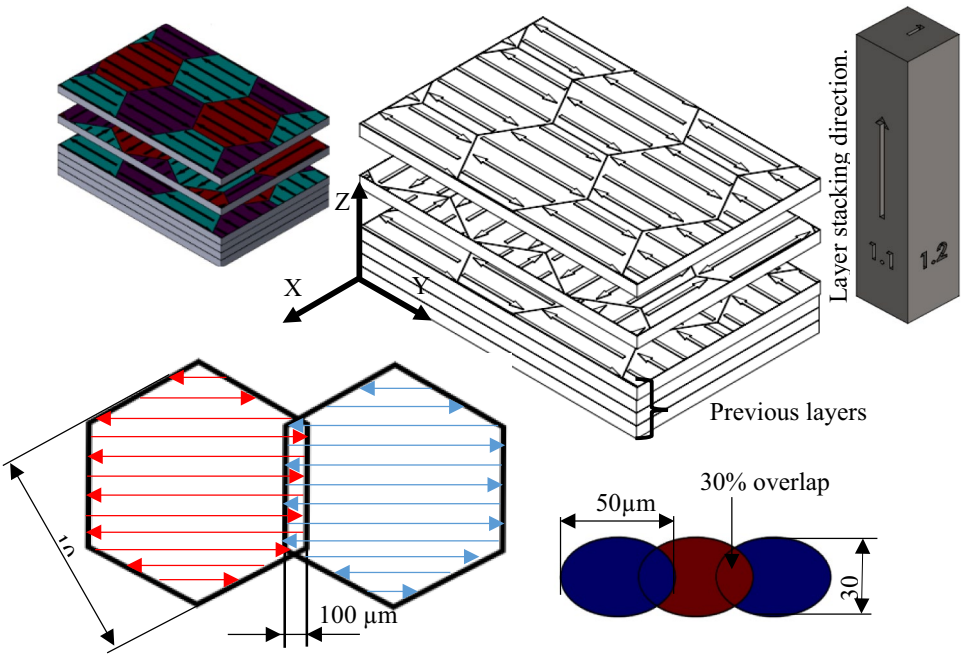

Fig. 1 Schematic representation of the scanning strategy employed in this study

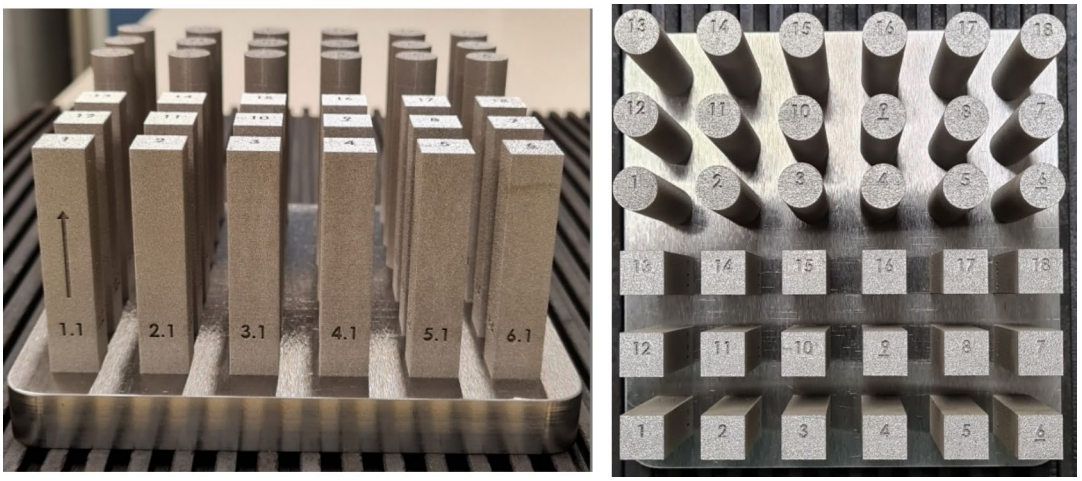

Fig. 2 Specimens of 17-4PH SS obtained by LPBF process

To identify and indicate for each specimen its position on the LPBF machine platform, a number ***i*** was marked on its upper surface (for the first specimen, $i=1$, and so for the others). The four sides of prismatic specimens were numbered from ***i.1*** to ***i.4*** allowing a unique identification. An arrow is indicated on the first specimen to mention the build-up direction, which signifies the direction in which layers were deposited during the LPBF manufacturing process (Fig. 2).

After LPBF fabrication and before the specimen's extraction, the entire assembly (specimens and platform) was subjected to a relaxing heat treatment at 760 °C for 2 h followed by air-cooling. This post-treatment prevents dimensional variations and deformations of specimens caused by stress relaxation after their separation from the platform. Afterwards, the specimens are extracted from the build platform using an electrical discharge machine (EDM) cutting. This technique allows for meticulous separation with high precision and without compromising the integrity of both the specimens and the platform.

2.3 Heat treatments

It is commonly accepted that the strength, hardness, toughness and corrosion resistance of 17-4PH martensitic precipitation hardened stainless steel are closely related to the aging process. Therefore, the aging conditions for this stainless steel are chosen based on the desired mechanical properties. Specifically, Mirzadeh et al. [24] and Pellegrini et al. [26] reported that aging of 17-4PH MSS at high temperatures (above 595 °C) and for holding times of up to 4 h generally leads to a softer material compared to other conditions (annealing, ageing at low temperatures, etc.). Indeed, it has been shown that super-aging conditions decrease hardness, reduce porosity [26], improve corrosion resistance and reduce the pitting potential [35]. Consequently, super-aging conditions were chosen to compare the microstructure and mechanical properties of LPBF and rolled 17-4PH MSS. The thermal treatment conditions considered and applied to both rolled and LPBF samples are presented in Table 3.

2.4 Microstructure characterization

Metallographic specimens cut from the LPBF and Rolled samples were prepared according to the standard technique. The examined surfaces were mechanically ground and electropolished. X-ray diffraction (Bruker D8 Advance) for phase identification and EBSD (HKL) measurements were directly performed on the electropolished surfaces. The microstructure was further examined on the electropolished and etched surface by an optical microscope (Olympus DSX1000) and a field emission SEM (ZEISS Gemini SEM 460). For the etching procedure, the electropolished surface was etched in Viella reagent (ASTM E 407 – 80 Viella) (100 ml ethanol, 5 ml hydrochloric acid, and 3 g picric acid) for 15 s.

Table 3 Considered states and heat treatment conditions for the studied 17-4PH SS

Considered states	LPBF	Rolled
S0: As received state	760 °C–2H–Air cooling	Under mill-annealed condition
S1: Solution annealing State	1050 °C–1H–Air cooling	
S2: Aging state	1050 °C–1H–Air cooling + 630 °C–4H–air cooling	

2.5 Mechanical characterization

Microhardness measurements were conducted using an FM-810 Microhardness Tester controlled by ARGO software. Before microhardness measurements, the samples ($10\times10\times10$ mm^3) were embedded in hot epoxy resin and then polished down to 2400 with SiC. Subsequently, they were meticulously rinsed and cleaned in ethanol using an ultrasonic bath and dried by airflow.

For each microhardness measurement, a load of 500gf was applied to the sample for an approximate duration of 10 s. This procedure was repeated on an array of 20 indentations, staggered and separated by an average distance of 500 µm (at least 10 times the diagonal of the indentation). Considering the errors associated with diagonal measurements and their repeatability, the uncertainty of the results provided by this microhardness tester, for a load of 500 gf, a $50\times$ objective, is approximately $\pm$ 30 HV.

Specimens were prepared, in accordance with ISO 6892-1984F, in the build-up direction of LPBF samples (Figs. 1 and 2) and in the rolling direction of rolled bar (Fig. 3a, b).

These specimens were machined using CNC turning, and the tensile test was carried out at room temperature (RT) under a quasistatic loading rate of 10 Mpa/s using a Zwick Roell 1475 universal testing machine.

The impact or Charpy V-Notch (CVN) energy absorption tests specimens were machined to dimensions of $10\times10\times55$ mm3 with a V-notch, created by EDM, with a depth of 2 mm and an angle of 45° (Fig. 3c). The impact tests were carried out on a Charpy FRANK pendulum machine equipped with two heads of 150 J and 300 J.

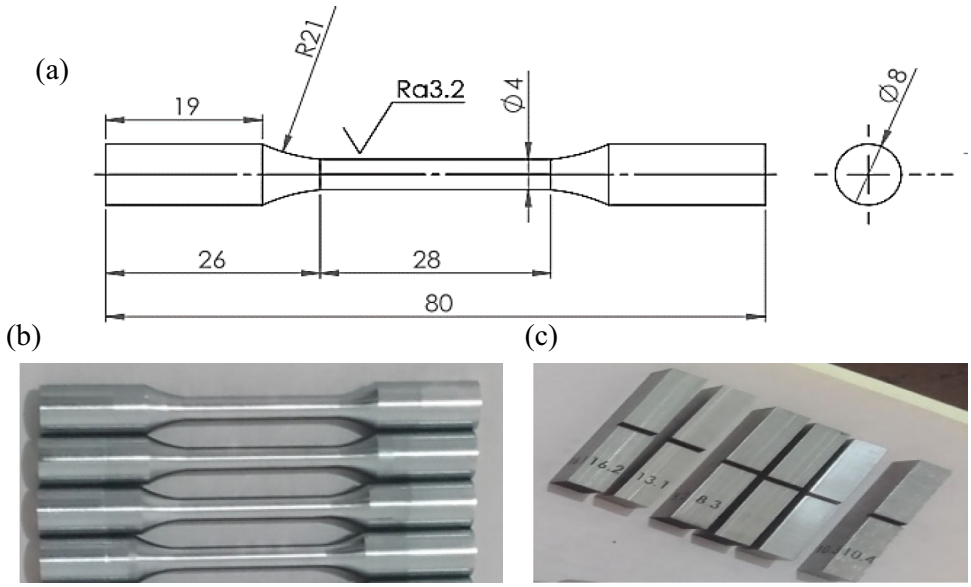

Fig. 3 Standard (**a**), **b** tensile and c resilience specimen tests (dimensions are expressed in mm)

3 Results and discussions

3.1 Microstructure of 17–4 PH SS

Figure 4 shows OM images that reveal significant microstructural differences between LPBF and Rolled 17-4PH MSS. The microstructure of LPBF 17-4PH is relatively fine, with pores and some non-metallic inclusions randomly distributed at the grain boundaries and within the grains, which is consistent with previous studies [16, 17, 31]. This is probably related to the local thermal melting-solidification cycle, extremely rapid (~ 10^6 K/S), complex and violent depending on the machine working parameters and powder characteristics Saboni et al. [29]. Additionally, during the LPBF process, the overlapped area of the adjacent layer is re-melted and re-solidified leading to the melting and recrystallization of the initial coarse grains in this zone. This results in a unique grain morphology with many bent grain boundaries presented in the microstructure of the LPBF sample.

Figure 5 shows that the matrix of the LPBF 17-4PH samples is primarily martensitic at all heat treatment states, as indicated by the XRD spectra. The same figure also shows that the martensite and austenite contents of Rolled 17-4PH samples vary significantly with the same applied heat treatment. These results were confirmed by analyzes of the phase constituents based on the EBSD measurements summarized in Table 4 and presented in Fig. 6 for the aged samples (S2 state). We note that, in Table 4, Zero solutions, also referred to as non-indexed solutions, represent the points in the scan for which no indexing solution could be found for the corresponding pattern. These results reveal that the content of the γ phase in in the three samples of considered states of LPBF 17-4PH is very limited. At received state, the rolled samples have a very high austenite content (14.7%) but after the solution annealing (S1), a disappearance of austenite and of other precipitates, and martensitic phase predominates, constituting approximately 98%. It is worth noting that the phase contents are identical for both LPBF and rolled samples after solution annealing. However, the aging heat treatment of the rolled samples (S2) led to a significant reappearance of austenite and other precipitates, which constitutes a notable difference compared to those fabricated by LPBF (Fig. 6). It is important to note that the 17-4PH MSS contains two types of austenite: residual and revert austenite. The ratio of martensite to austenite has a significant impact on the mechanical, physicochemical properties, and in-service behavior of these steels [2, 15, 37].

Microstructure results for LPBF parts at the as-received states are in agreement with the majority of work available in the literature [7, 9, 11, 22, 38]. The results of microstructural evolution after heat treatments are consistent with those of Hasbrouck et al. (2023) and Moyle et al. [25] for the Low N 17-4PH. For different LPBF manufacturing conditions, these results are contradicted by other previous studies, which showed that aging heat treatment results in a microstructure similar to that of samples obtained by traditional manufacturing methods [7, 22]. This justifies that the parameters and conditions of LPBF manufacturing process play a crucial role not only on the microstructure obtained during manufacturing but also on its evolution during the post-processing treatments. Thus, the adaptation of the mechanical properties of 17-4PH samples manufactured by LPBF requires the optimization of the process parameters, strategy of fabrication, the exploitation of thermal cycles specific to the process and the exploration of new heat post-treatments.

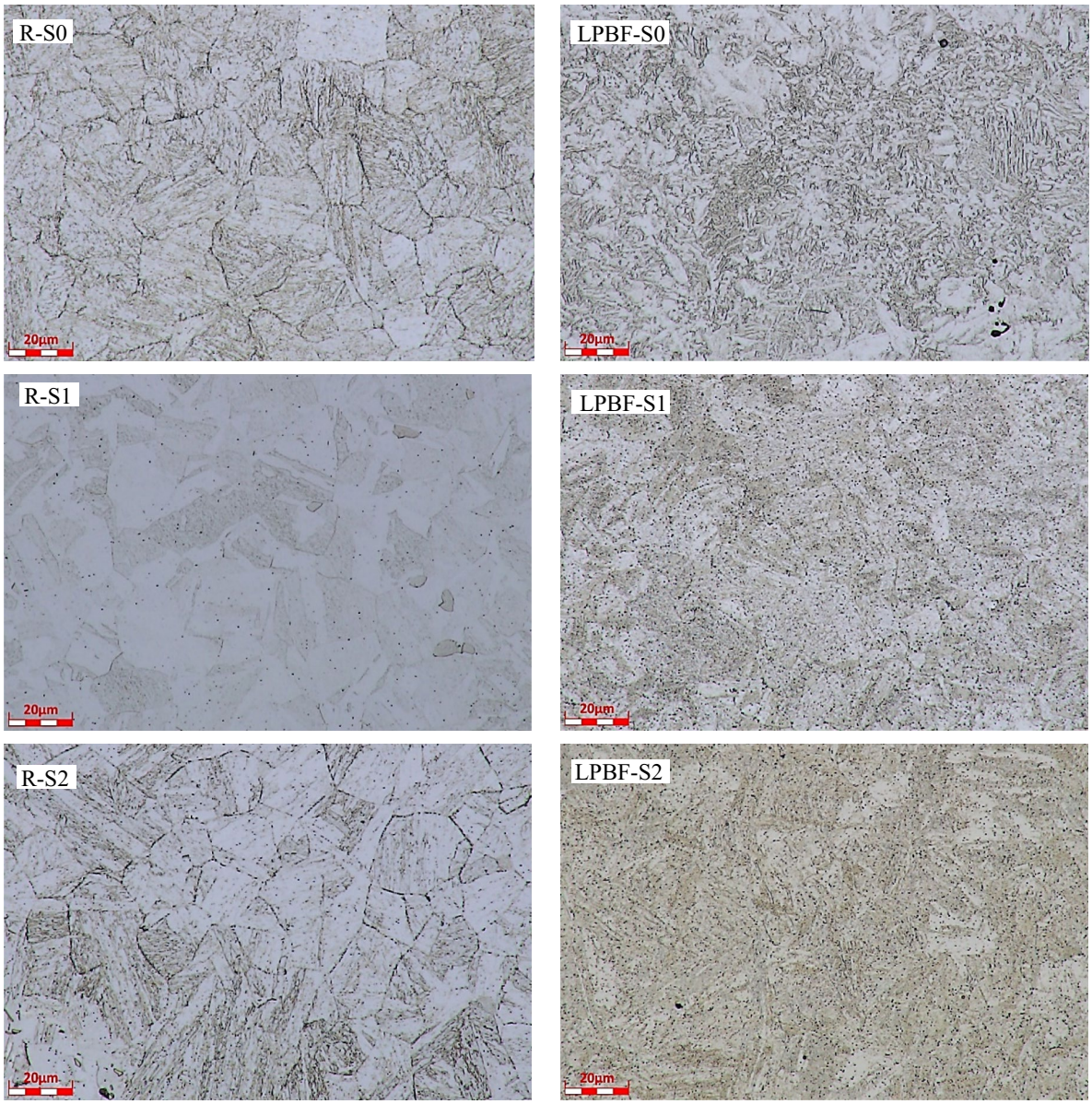

(a) Rolled samples (b) LPBF samples

Fig. 4 Optical microscope image of the **a** Rolled and **b** LPBF 17-4PH MSS samples

Moreover, the results indicate the presence of unidentified precipitates in all states of rolled and LPBF samples with a significant fraction ranging and a complex composition. Additionally, defects in the form of pores, unmelted powder, and delamination are observed in the LPBF samples.

The precipitates, which appear, as a mixture of inclusions, oxides, and pores, in LPBF samples, require in-depth analysis to better understand their impact on the mechanical and physicochemical properties of obtained steel. Figures 7, 8 and Table 5 display the EDX microanalysis results for these precipitates. They reveal that the pores represent zones of agglomeration of components such as O, Si, S, Nb, and Mn and an ultimately localized nucleation of detrimental precipitates leading to creation of Fe, Cr, and Ni denuded zones near the pores and consequently the embrittlement and corrosion resistance degradation of material.

3.2 Microhardness

The results of microhardness measurements of 17-4PH SS powder at the as-received state, and rolled at the three considered states, and LPBF in the laser-scanning plane (XY) and along the building direction (Z) (Fig. 2) at the three considered states are given in Fig. 9.

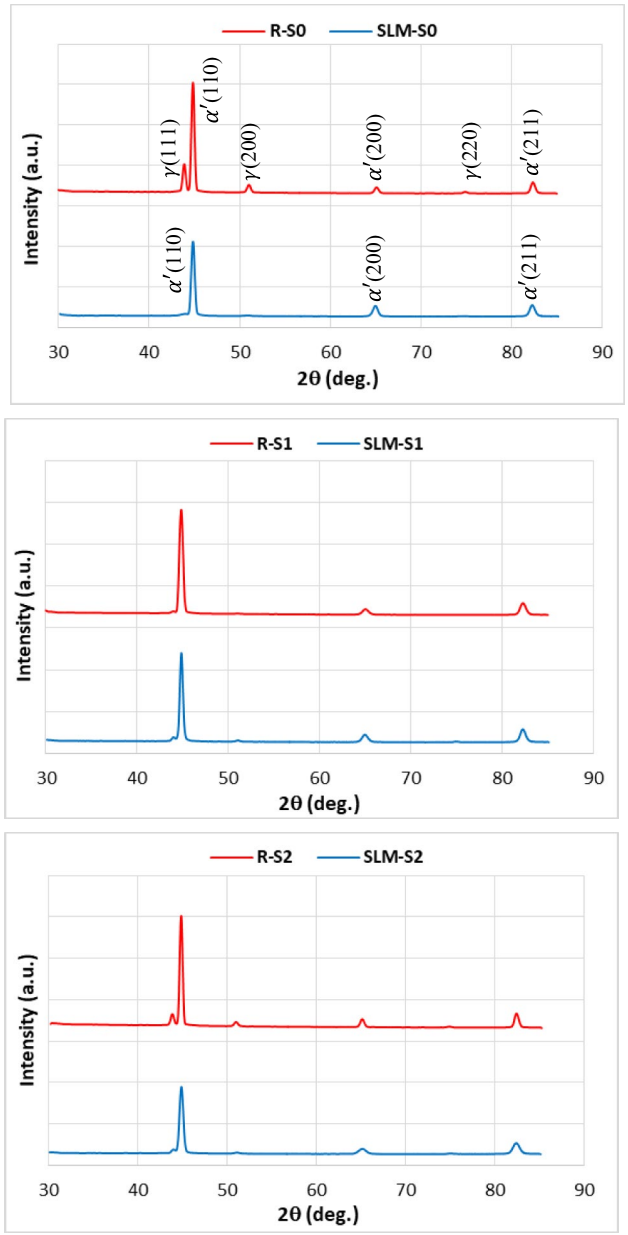

Fig. 5 XRD spectra of the rolled and LPBF 17–4 PH MSS samples

Table 4 Results of ESBD calculations of the phases distribution in the three considered states of the Rolled and LPBF 17-4PH MSS samples

Process	State	Martensite $\alpha\prime$ (%)	Austenite γ (%)	Zero solutions (%)
LPBF	S0	94.05	0.14	5.81
	S1	97.28	0.07	2.65
	S2	97.39	0.06	2.55
Rolling	S0	81.12	14.70	4.18
	S1	98.10	0.05	1.85
	S2	90.08	3.98	5.94

Following the LPBF process the results show, in agreement with AlMangour et al. [1], that the microhardness of 17-4PH increases due to the powder's melting and consolidation. At the S0 state, the rolled 17-4PH SS exhibits a relatively lower microhardness of the LPBF. This is explained by the rapid melting and solidification during the LPBF process, resulting in the formation of a fine microstructure compared to the one obtained by rolling process [6, 14, 31]. The microhardness evolves similarly after heat treatments while keeping a superiority discard for the LPBF 17-4PH. The microhardness decreases slightly after the solution annealing heat treatment (S1) can be attributed to the relaxation of residual stresses. However, it increases, as expected, after aging treatment, reaching averages values of 420HV0.5 for LPBF and 350HV0.5 for rolled 17-4PH SS. This is attributed to the precipitation phenomenon, which should occur during the aging of this type of structural hardening materials.

Furthermore, as shown in Fig. 9, the variation in the average microhardness values is minimal between the two manufacturing orientations of LPBF (XY and XZ). Nevertheless, it is important to note that, when measuring the microhardness according to the direction of construction (Z), a drop was observed in certain zones, which probably correspond to the interlayer's cohesion defects. These measurements have been discarded in the calculation of the average values given by Fig. 9. In addition, a small gap was observed between the base and the head of the specimen in the S0 state, which almost disappeared after solution heat and aging treatments (S1 and S2 states). These gaps are the typical consequences of the thermal cycles associated at additive manufacturing by LPBF. This can be underlined particularly with rapid cooling of local melted powders on a relatively cold substrate or on previously deposited layers with a significant temperature difference.

3.3 Tensile strength

For each state, measurements were carried out three times to obtain the average values and ranges of given mechanical properties. The obtained results are given by the stress–strain curves (Fig. 10) of LPBF and rolled 17-4PH SS under proposed states (S0, S1, and S2). Other results concern the SEM micro-fractography operated on the fracture facies of the broken parts are illustrated by Fig. 11. The mechanical properties deducted for the different tested conditions are also presented in Table 6.

It can be concluded that the solution heat and aging treatments improves noticeable the ultimate tensile strength σ_{UTS} of LPBF 17-4PH SS. Indeed, the ultimate strength increases from around 1030 MPa for the S0 state to around 1060 MPa after the solution annealing heat treatment (S1 condition), and further to 1230 MPa after the aging treatment (S2 condition). The improvement

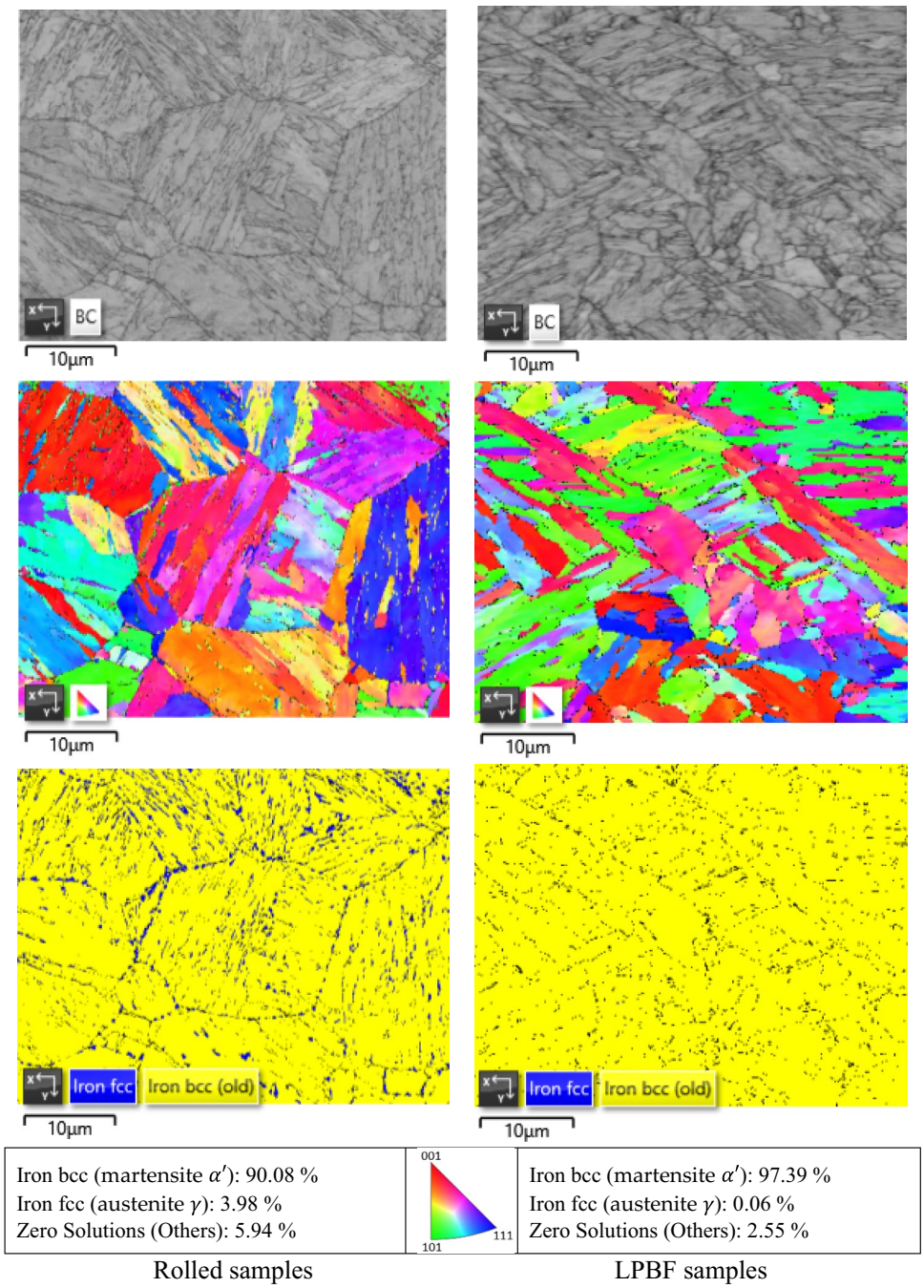

Fig. 6 EBSD characterizations of the aged samples (S2 state) of LPBF and rolled 17–4 PH MSS: Band Contrast (BC) images are shown in the first row, IPF maps in the second row, and phase maps in the third row (Yellow phase is bcc (martensite $\alpha\prime$), Blue phase is fcc (austenite γ), and black points represent zero solutions)

in the elongation at fracture of LPBF 17-4PH SS after annealing and aging heat treatments cannot be considered as significant. Initially, around 2.3% for the S0 state, it evolved to 3% after the solution annealing heat treatment (S1 condition) and less to 2% after the aging treatment (S2 condition). The considered heat treatment conditions do not manage to increase the ductility of the LPBF 17-4PH SS parts. Indeed, the stress–strain curves clearly show the lower ductility of LPBF 17-4PH SS, as the points of maximum resistance (σ_{UTS}) align with the elongation at failure (El%). The micro-fractography analysis of LPBF 17–4 PH considered states also shows the brittle fracture phenomenon that occurred generally under transgranular cleavage and coalescence of cavities (Fig. 11a, b and c). These results are consistent with those of Auguste et al. [3] who found elongations of less than 3% for the as-received state (AsB) and for the aging states comparable to ours (SHT-T480 and H-SHT-T480). Thy corroborate also with those found by Vilaro et al. [36] who found that the ductility of the longitudinal and transverse directions of LPBF Ti–6Al–4 V alloys are respectively 7.6% and 1.7% (35%

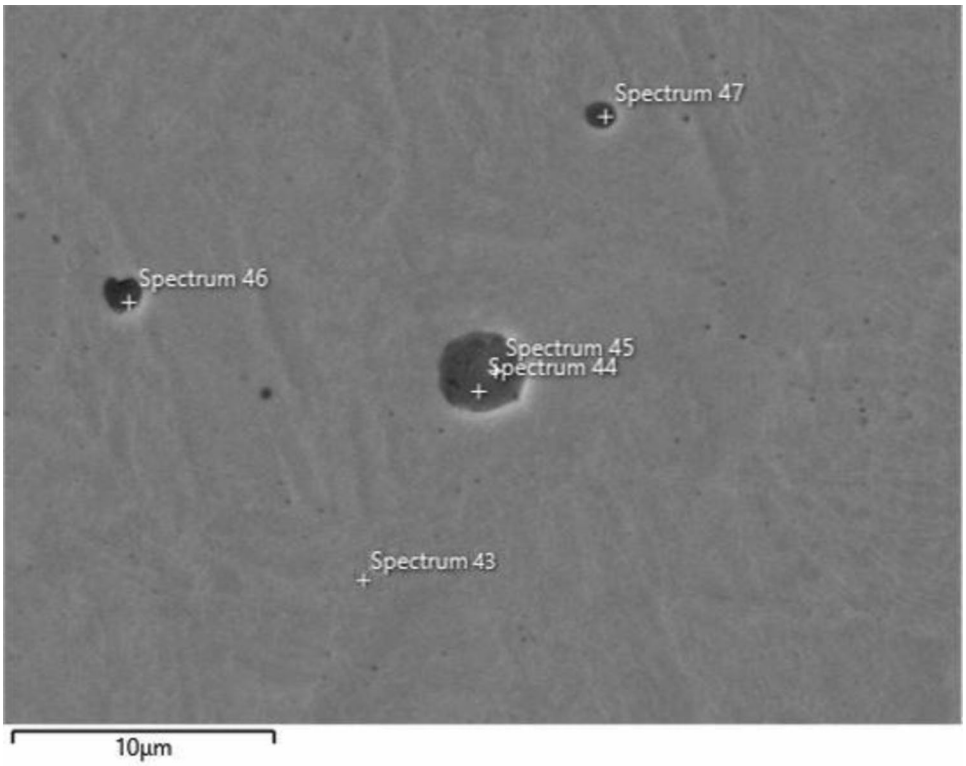

Fig. 7 Spectrum locations on the sample section of the S2 state of LPBF 17-4PH MSS

of ductility anisotropy) but the ultimate tensile strengths (UTS) of these two directions were comparable.

The rolled 17-4PH MSS exhibits an elongation at fracture, around 17.5%, much more important than LPBF with a slightly lower ultimate tensile strength (around 1000 MPa). This difference can principally be attributed to the homogeneous microstructure of the rolled 17-4PH MSS with the total absence of porosities and cavities. In addition, aging treatment allows to confer, as expected, optimal mechanical properties to the rolled 17-4PH SS as showed by Fig. 10. Indeed, the ultimate tensile strength increases after the aging treatments, reaching an average of 1060 MPa while keeping an elastic strength around 900 MPa and an elongation at the fracture more than 16%.

The rolled 17-4PH exhibits a higher yield strength in all considered heat treatment states. Additionally, yield strength decreases for both steels after the solution annealing and the aging heat treatment, when passing from 904 and 714 MPa at S0-state to 879 MPa and 685 MPa at aging state (S2) respectively for rolled and LPBF 17-4PH. This difference can be attributed to the large difference in martensite and austenite contents in the rolled and LPBF samples as well as defects such as pores, inclusions, and detrimental precipitates in the LPBF samples.

For all considered states, the SEM micro-fractography of tensile fracture surfaces of LPBF samples reveals different kinds of defects, resulting from the AM process. This leads to a more susceptible microstructure to failure. According to the literature [5, 32, 34, 37], notable observed defects are pores with varying sizes and shapes, microcracks, partially or unmelted grains, projected particles, and concentrated oxide inclusions at the center of cupules (Fig. 11a, b and c).

The observed fracture surfaces exhibit significant irregularities due to the presence of porosity. The micro-fractographies illustrate the presence of cupules in different sizes, along with cleavage rivers, indicating mixed fractures in narrow regions following the solution annealing and aging process (Fig. 11b and c). The formation of these cupules can be attributed to the nucleation and coalescence of micro-voids in regions with localized deformation discontinuities.

In the magnified area of Fig. 11b and c, tiny particles ranging in size from 10 to 100 nm can be observed. Their small size rules out their possibility to be unfused powder particles, but rather oxide inclusions (SiO_2). According to Gupta et al. [12], it has been demonstrated that these oxide inclusions in the steel could initiate crack formation due to the concentration of internal stresses around them, resulting in a deterioration of ductility. Therefore, in addition to pores and improper powder layer fusion, the formation of oxide inclusions is considered one of the causes of decreased ductility.

It should be noted that the surface of the cupules in the traction fracture zones of rolled 17-4PH SS increases after the heat treatments. It varies from about 11 μm^2 in the S0 state to about 37 μm^2 and 165 μm^2 for the S1 and S2 states (Fig. 11d, e and f), respectively. Nevertheless, these cupules

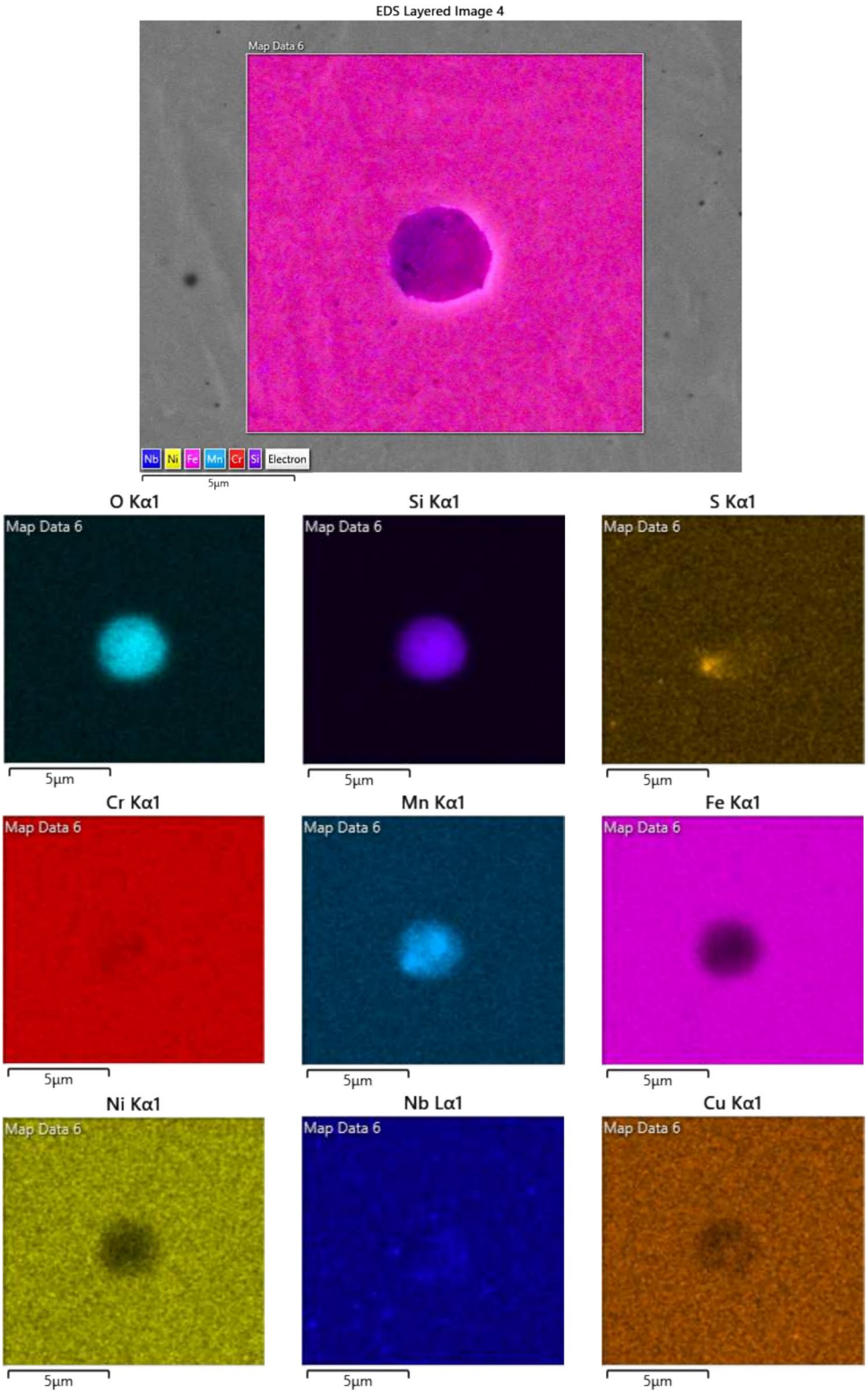

Fig. 8 X-ray maps of the major chemical components inside and around the pores for the S2 state of LPBF 17-4PH

are hardly visible on the surface of the fracture zones of LPBF parts (Fig. 11a, b and c). They appear in narrow and small areas of approximately 1 to 2µm^2 at the S1 state and they expand to around 3 to 4 µm^2 following the aging treatment (S2 state).

Obtained results are in agreement with the results of the microstructural analysis, which revealed a martensitic microstructure of LPBF parts offering high hardness (+ 20% of $HV_{0.5}$) and ultimate tensile strength (+ 15% of UTS) against low elastic strength (- 28% of YTS) and

Table 5 Chemical composition (Wt.%) of the S2 state of LPBF 17-4PH MSS based on EDS microanalysis

Spectrum	Si	Mn	Ni	Cr	Cu	Nb	S	O	Fe
43 (matrix)	0.66	0.61	4.56	17.13	3.60	0.25	0.09	0.73	72.37
44	13.28	8.01	1.80	17.81	2.88	1.48	0.60	22.73	31.41
45	14.84	13.71	1.18	15.80	3.03	2.10	0.10	25.75	23.49
46	9.28	6.03	2.63	17.14	3.12	1.08	0.24	14.96	45.52
47	7.02	4.33	2.74	18.96	3.01	1.48	0.02	12.63	49.81

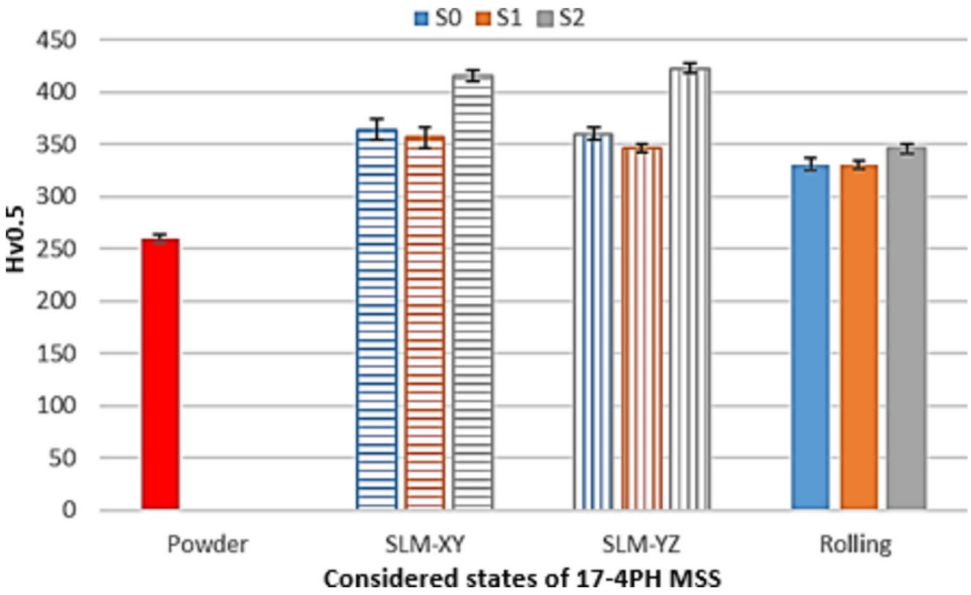

Fig. 9 Average microhardness Hv0.5 of 17-4PH MSS at the considered states

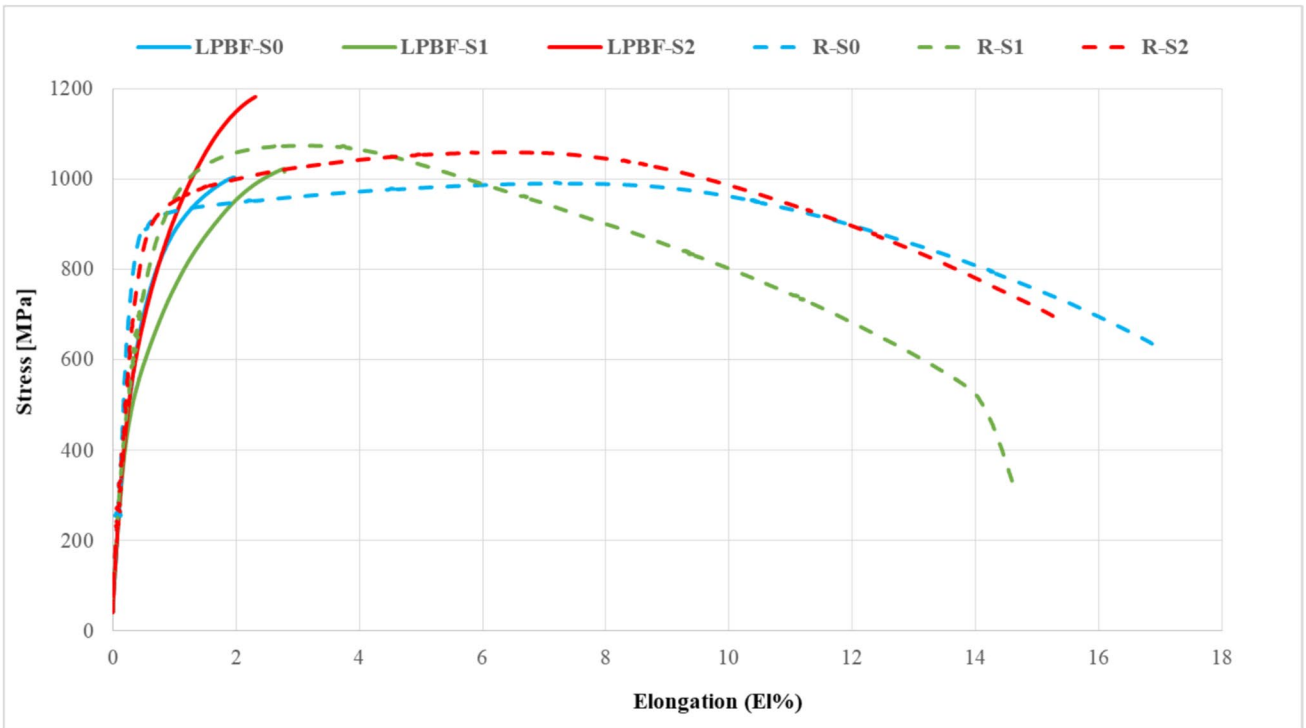

Fig. 10 Stress–elongation curves of the LPBF and rolled 17-4PH SS at considered states

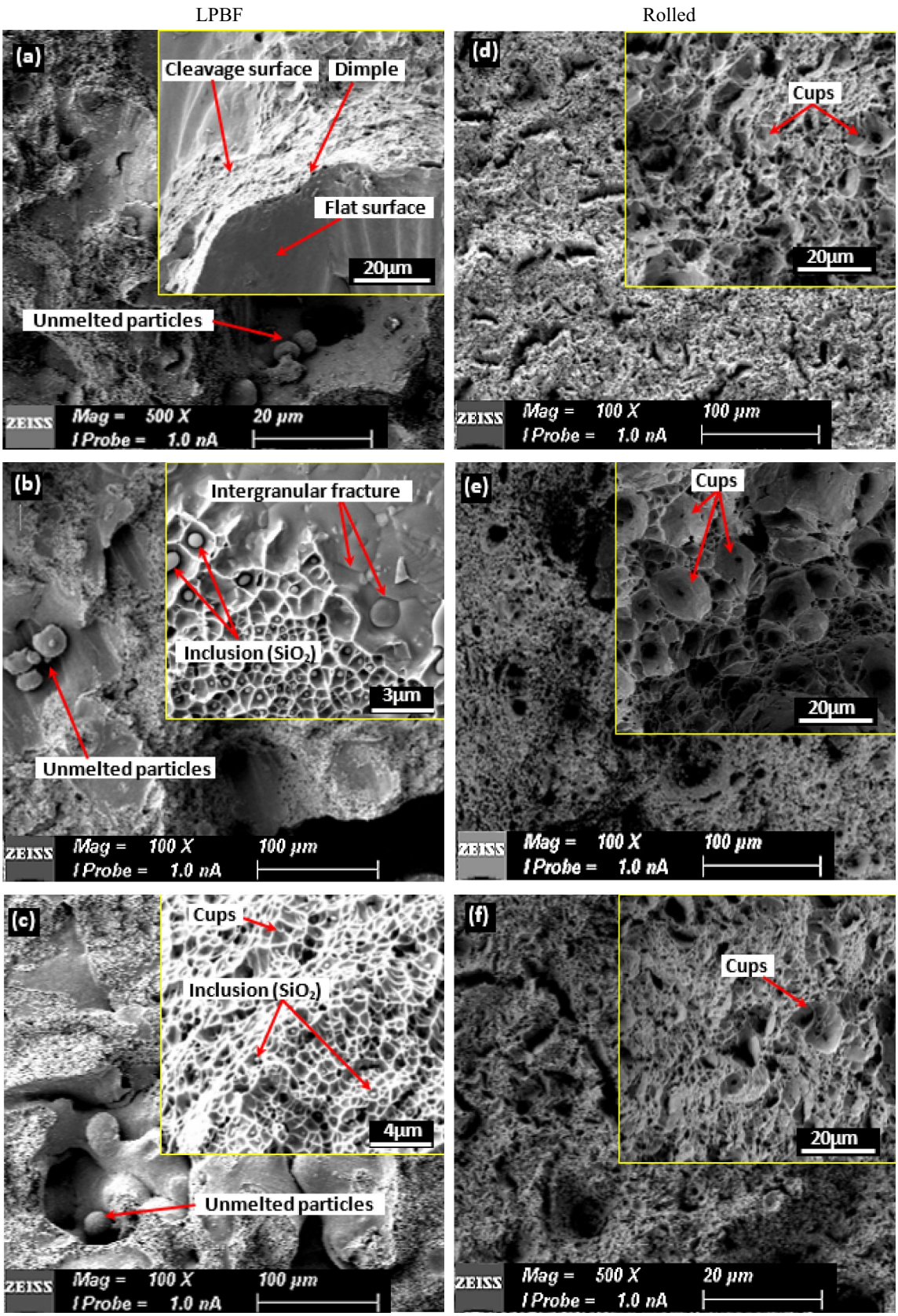

Fig. 11 SEM microfractography of LPBF and rolled 17-4PH SS at respectively considered states: S0: (**a**) and (**d**), S1: (**b**) and (**e**), S2: (**c**) and (**f**)

Table 6 Summarized mechanical properties obtained by tensile test on LPBF and Rolled 17-4PH SS at considered states

		σ_{Ys}(MPa)	σ_{UTS}(MPa)	El (%)
LPBF	LPBF-S0	714 ± 55	1030 ± 56.0	1.9 ± 0.6
	LPBF-S1	557 ± 18	1057 ± 29.0	3.7 ± 1.0
	LPBF-S2	685 ± 35	1226 ± 17.0	2,1 ± 0.2
Rolling	Rolled-S0	904 ± 17	992 ± 33.0	17.5 ± 0.3
	Rolled-S1	726 ± 58	1077 ± 1.4	14.6 ± 0.1
	Rolled-S2	879 ± 54	1063 ± 12.0	16 ± 0.1

Table 7 Average value of resilience K of the LPBF and Rolled 17-4PH-SS

17-4PH Sate Sample	K- LPBF (J/cm2)	K- Rolled (J/cm2)	Rate(%)
S0	11	95	88
S1	12.5	150	92
S2	11	155	93

ductility (−66% of El%). Unlike hard and brittle martensite, austenite is a soft and ductile phase and its presence gives the rolled part greater ductility.

3.4 Impact toughness

Results of the Charpy V-Notch tests carried out on LPBF and rolled 17-4PH-SS under considered states S0, S1 and S3 are given in Table 7. The results of optical fractography operates on the fracture facies of the broken parts are illustrated by Fig. 12. We underline the very week impact-resistance (resilience K) of the LPBF 17-4PH which is around 11 J/cm^2 against 95 J/cm^2 for the rolled parts at the S0 state. This difference, which represents a rate of around 88% at the S0 state, extends out to a rate of 93% after aging heat treatment (S2 state). This great difference is principally attributed to the presence of defects and the nucleation of embrittlement precipitates in LPBF samples as confirmed previously by microstructural microanalysis and by the micrographic's examination of the fracture surfaces (Fig. 12a, b and c). These results are in agreement with those found by a few works in the literature; e.g., Riza et al. [28] found that the max value of impact toughness of 17-4PH LPBF specimens was nearly 30 J at room temperature and they consider that the value is significantly lesser than the similar type of wrought steels as found in material properties literature.

The heat treatment did not increase the low impact resistance of LPBF 17-4PH SS unlike rolled parts where the resilience increases from 95 J/cm^2 to 155 J/cm^2 after the aging treatment (S2). Therefore, the inherent weakness

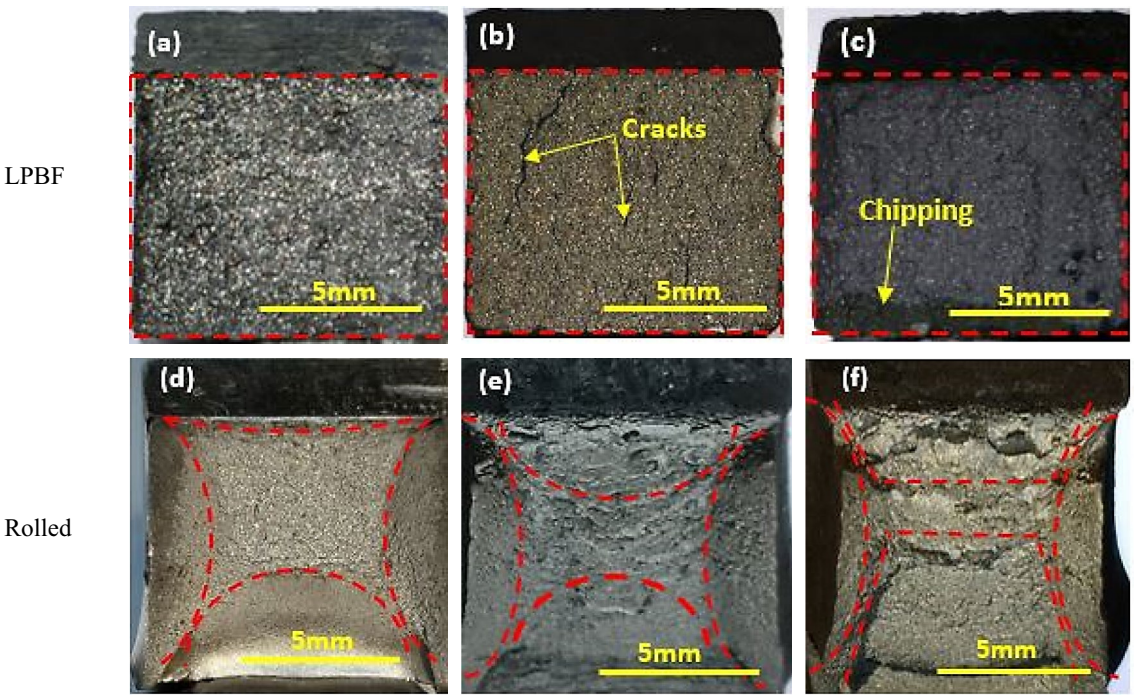

Fig. 12 Optical fractography after Charpy impact tests of **a** S0, **b** S1 and **c** S2 of LPBF Sample, **d** S0, **e** S1 and **f** S2 of rolled samples

and non-homogeneity of microstructure induced by LPBF process were not efficiently cured.

Practically, it can be underlined no zones of impact resistance or plastic deformation in the three states of the LPBF samples (Fig. 12a, b and c). However, we notice the presence of macroscopic cracks with a length of 5 mm (Fig. 12b) and separation or chipping of the material in the fracture zone (Fig. 12c). The results are consistent with the study conducted by Lou et al. [19], which showed that the impact toughness of AM materials is relatively very low with a rate of approximately 63% compared to that of wrought materials. They also confirm that pores, particles, and Mn, Mo, and Si-rich precipitates lead to the degradation of impact strength.

A zone of impact resistance, ranging with plastic deformation from 60 to 80%, is observed in the case of rolled 17-4PH SS parts. The striction zone developed after the annealing and aging heat treatment, indicates the benefit of these post-treatments on the mechanical properties of the rolled 17-4PH, unlike the LPBF 17-4PH where the heat treatment did not show no significant effect on impact resistance (Fig. 12d, e and f).

It is very important to note that Ming et al. [23], studying the impact resistance of LPBF Ti-6Al-4 V, found that although the relative density is greater than 99.5% and although it is the same for Vertical and Horizontal samples, the impact energy of the as-built samples was low and that of H-sample was 96% higher than that of V-sample (4.9 J vs. 9.6 J). These findings demonstrate that the building direction strongly affects the impact property of LPBF parts and structure but does not affect the relative density.

The remarkable difference in the studied mechanical properties is attributed to the inherent micro- and macro-structural differences related to the appropriate thermal histories to each one of the concerned processes. Indeed, it has been well approved that additive manufacturing by LPBF generates various defects, morphology and roughness [30, 33], cohesion between layers [15], pores [5, 27], unmelted powders [18], residual stresses [2, 20]. Whereas the samples obtained by rolled process have a fully dense structure, negligible residual stress, and favorable grain orientation.

It is also important to underline that the aging treatment, often used to improve the mechanical properties of the martensitic precipitation hardening stainless steels and which has shown its efficacy in the case of rolled 17-4PH SS, has not any effect on the mechanical properties of LPBF 17-4PH SS specimens. It is, therefore, essential to develop new and appropriate post-treatments allowing to reduce manufacturing defects improving the ductility and optimizing the mechanical properties of LPBF 17-4PH SS. It is also possible to reduce the undesirable effects by the optimization of process parameters and by the control and exploitation of specific thermal cycles during fabrication by LPBF process.

4 Conclusion

Mechanical properties of LPBF and rolled 17-4PH MSS samples were compared for three treatments conditions states, as received, solution annealed and aging treatment. The main conclusions are summarized as follows:

- Significant microstructural differences between LPBF and rolled 17-4PH MSS. The microstructure of LPBF 17-4PH is relatively fine, with pores and some non-metallic inclusions randomly distributed at the grain boundaries and within the grains.
- The aging heat treatment, which is commonly used to enhance the mechanical properties and corrosion resistance to the 17-4PH MSS obtained by traditional processes, appears to be unsuitable for those obtained through LPBF. This is likely due to the defects and pores generated by the LPBF process, which can serve for the localized nucleation of detrimental precipitates, ultimately leading to the embrittlement of the obtained material.
- Compared to rolled 17-4PH, the LPBF one exhibit slightly higher microhardness, mechanical resistance, but lower elongation at fracture and weaker impact resistance. Failure in LPBF samples is operated by cleavage and coalescence of cavities, whereas rolling ones demonstrate a progressive failure mechanism driven by plasticity and damage evolution.
- The higher microhardness, ultimate tensile strength of LPBF samples are mainly attributed to the fine martensitic microstructure generated by the rapid melting and solidification during the LPBF process.
- The high impact resistance and significant difference in ductility of rolled 17-4PH MSS can be attributed to its fully dense microstructure and favorable grain orientation. Moreover, unlike hard and brittle martensite, austenite is a soft and ductile phase and its presence gives the rolled part greater ductility.
- Reducing manufacturing defects and adapting of the mechanical properties of 17-4PH samples manufactured by LPBF requires the optimization of the manufacturing parameters, strategy and conditions, the exploitation of thermal cycles specific to the process and the exploration of new heat post-treatments.

Acknowledgements The authors acknowledge the financial support of the State Secretariat for Education, Research and Innovation (SERI)—Switzerland, through the Research Partnership Grants 2022 of the

Leading House for the Middle East and North Africa Region (MENA) commissioned to HES-SO.

Funding Open access funding provided by University of Applied Sciences and Arts Western Switzerland (HES-SO). This work was supported by the Haute école Spécialisée de Suisse Occidentale.

Data availability The data that support the findings of this study are available from the corresponding author upon reasonable request.

Declarations

Conflict of interest All authors certify that they have no affiliations with or involvement in any organization or entity with any financial interest or non-financial interest in the subject matter or materials discussed in this manuscript.

References

1. AlMangour B, Yang J-M (2016) Improving the surface quality and mechanical properties by shot-peening of 17–4 stainless steel fabricated by additive manufacturing. Mater Des 110:914–924. https://doi.org/10.1016/j.matdes.2016.08.037
2. Andreacola FR, Capasso I, Pilotti L (2021) Brando G Influence of 3D-printing parameters on the mechanical properties of 17–4PH stainless steel produced through Selective Laser Melting. Frattura ed Integrità Strutturale. https://doi.org/10.3221/IGF-ESIS.58.21
3. Auguste P, Mauduit A, Fouquet L, Pillot S (2018) Study on 17–4 PH stainless steel produced by selective laser melting. UPB Scient Bull Series B Chem Mater Sci 80:197–210
4. Bertocco A, Iannitti G, Caraviello A, Esposito L (2022) Lattice structures in stainless steel 17–4PH manufactured via selective laser melting (SLM) process: dimensional accuracy, satellites formation, compressive response and printing parameters optimization. Int J Adv Manuf Technol 120:4935–4949. https://doi.org/10.1007/s00170-022-08946-2
5. Carlton HD, Haboub A, Gallegos GF, Parkinson DY, MacDowell AA (2016) Damage evolution and failure mechanisms in additively manufactured stainless steel. Mater Sci Eng A 651:406–414. https://doi.org/10.1016/j.msea.2015.10.073
6. Chang SJ, Wei ZX (2022) Influences of the scanning strategy on surface roughness in selective laser melting. Proc Inst Mech Eng Part B J Eng Manuf 236:1853–1866. https://doi.org/10.1177/0954405420978119
7. Choo W, Ebrahimian M, Choi K, Kim JH (2023) Influence of heat treatment on the microstructure and hardness of 17–4PH stainless steel fabricated through direct energy deposition. Met Mater Int 29:1750–1760. https://doi.org/10.1007/s12540-022-01333-2
8. Etter T, Kunze K, Geiger F, Meidani H (2015) Reduction in mechanical anisotropy through high temperature heat treatment of Hastelloy X processed by Selective Laser Melting (SLM). IOP Conf Ser Mater Sci Eng 82:012097. https://doi.org/10.1088/1757-899X/82/1/012097
9. Eisazadeh H, Khadka S, Wang X et al (2024) A comparative study of the mechanical characteristics of additively and conventionally fabricated 17–4 precipitation hardened stainless steel. Prog Addit Manuf. https://doi.org/10.1007/s40964-024-00591-3
10. Feng Q, Tang Q, Liu Z, Liu Y, Setchi R (2018) An investigation of the mechanical properties of metallic lattice structures fabricated using selective laser melting. Proc Inst Mech Eng Part B J Eng Manuf 232:1719–1730. https://doi.org/10.1177/0954405416668924
11. Garcia CC, Hernández CG, Castro-Sastre MA, Fernandez-Abia AI, Rodriguez-Mendez ML, Martin-Pedrosa F (2023) Heat treatments of 17–4 PH SS processed by SLM to improve its strength and biocompatibility in biomedical applications. J Mater Res Technol 26:3524–3543. https://doi.org/10.1016/j.jmrt.2023.08.104
12. Gupta A, Goyal S, Padmanabhan KA, Singh AK (2015) Inclusions in steel: micro–macro modelling approach to analyse the effects of inclusions on the properties of steel. Int J Adv Manuf Technol 77:565–572. https://doi.org/10.1007/s00170-014-6464-5
13. Hsiao CN, Chiou CS, Yang JR (2002) Aging reactions in a 17–4 PH stainless steel. Mater Chem Phys 74:134–142. https://doi.org/10.1016/S0254-0584(01)00460-6
14. Jia Q, Zhang F, Rometsch P, Li J, Mata J, Weyland M, Bourgeois L, Sui M, Wu X (2020) Precipitation kinetics, microstructure evolution and mechanical behavior of a developed Al–Mn–Sc alloy fabricated by selective laser melting. Acta Mater 193:239–251. https://doi.org/10.1016/j.actamat.2020.04.015
15. Kedziora S, Decker T, Museyibov E, Morbach J, Hohmann S, Huwer A, Wahl M (2022) Strength properties of 316L and 17–4 PH stainless steel produced with additive manufacturing. Materials 15:6278. https://doi.org/10.3390/ma15186278
16. Lee HJ, Dao VH, Ma YW, Yu JM, Yoon KB (2020) Effects of process parameters on the high temperature strength of 17–4PH stainless steel produced by selective laser melting. J Mech Sci Technol 34:3261–3272. https://doi.org/10.1007/s12206-020-0718-y
17. Leo P, D'Ostuni S, Perulli P, Castro Sastre MA, Fernández-Abia AI, Barreiro J (2019) Analysis of microstructure and defects in 17–4 PH stainless steel sample manufactured by Selective Laser Melting. Procedia Manuf 41:66–73. https://doi.org/10.1016/j.promfg.2019.07.030
18. Li C, Liu D, Liu G, Liu S, Jin X, Bai Y (2023) Surface characteristics enhancement and morphology evolution of selective-laser-melting (SLM) fabricated stainless steel 316L by laser polishing. Opt Laser Technol 162:109246. https://doi.org/10.1016/j.optlastec.2023.109246
19. Lou X, Andresen PL, Rebak RB (2018) Oxide inclusions in laser additive manufactured stainless steel and their effects on impact toughness and stress corrosion cracking behavior. J Nucl Mater 499:182–190. https://doi.org/10.1016/j.jnucmat.2017.11.036
20. Masoomi M, Shamsaei N, Winholtz RA, Milner JL, Gnäupel-Herold T, Elwany A, Mahmoudi M, Thompson SM (2017) Residual stress measurements via neutron diffraction of additive manufactured stainless steel 17–4 PH. Data Brief 13:408–414. https://doi.org/10.1016/j.dib.2017.06.027
21. Mercelis P, Kruth J (2006) Residual stresses in selective laser sintering and selective laser melting. Rapid Prototyp J 12:254–265. https://doi.org/10.1108/13552540610707013
22. Merlin M, Morales C, Ferroni M, Fortini A, Soffritti C (2024) Influence of heat treatment parameters on the microstructure of 17–4 PH single tracks fabricated by direct energy deposition. Appl Sci 14:700. https://doi.org/10.3390/app14020700

23. Ming WW, Pang HL, Jhewn KC (2016) Anisotropy in the impact toughness of selective laser melted Ti–6Al–4V alloy. Mater Sci Eng, A 650:295–299. https://doi.org/10.1016/j.msea.2015.10.045
24. Mirzadeh H, Najafizadeh A (2009) Aging kinetics of 17–4 PH stainless steel. Mater Chem Phys 116–1:119–124. https://doi.org/10.1016/j.matchemphys.2009.02.049
25. Moyle MS, Haghdadi N, Theska F, Haines MP, Liao XZ, Ringer SP, Primig S (2024) Effect of compositional variations on the heat treatment response in 17–4 PH stainless steel fabricated by laser powder bed fusion. Mater Charact 209:113768. https://doi.org/10.1016/j.matchar.2024.113768
26. Pellegrini A, Lavecchia F, Guerra MG et al (2023) Influence of aging treatments on 17–4 PH stainless steel parts realized using material extrusion additive manufacturing technologies. Int J Adv Manuf Technol 126:163–178. https://doi.org/10.1007/s00170-023-11136-3
27. Pragana JP, Pombinha P, Duarte VR, Rodrigues TA, Oliveira JP, Bragança IM, Santos TG, Miranda RM, Coutinho L, Silva CM (2020) Influence of processing parameters on the density of 316L stainless steel parts manufactured through laser powder bed fusion. Proc Inst Mech Eng Part B J Eng Manuf 234:1246–1257. https://doi.org/10.1177/0954405420911768
28. Riza SH, Ashok AM, Masood SH, Sbarski I (2017) Sub-zero temperature effect on impact properties of 17–4PH stainless steel processed by selective laser melting. SSP 266:3–7. https://doi.org/10.4028/www.scientific.net/ssp.266.3
29. Sabooni S, Chabok A, Feng SC, Blaauw H, Pijper TC, Yang HJ, Pei YT (2021) Laser powder bed fusion of 17–4 PH stainless steel: A comparative study on the effect of heat treatment on the microstructure evolution and mechanical properties. Addit Manuf 46:102176. https://doi.org/10.1016/j.addma.2021.102176
30. Sadali MF, Hassan MZ, Ahmad F, Yahaya H, Rasid ZA (2020) Influence of selective laser melting scanning speed parameter on the surface morphology, surface roughness, and micropores for manufactured Ti6Al4V parts. J Mater Res 35:2025–2035. https://doi.org/10.1557/jmr.2020.84
31. Sghaier TAM, Sahlaoui H, Mabrouki T, Sallem H, Rech J (2023) Selective laser melting of stainless-steel: a review of process, microstructure, mechanical properties and post-processing treatments. Int J Mater Form 16:41. https://doi.org/10.1007/s12289-023-01769-w
32. Shi Q, Qin F, Li K, Liu X, Zhou G (2021) Effect of hot isostatic pressing on the microstructure and mechanical properties of 17–4PH stainless steel parts fabricated by selective laser melting. Mater Sci Eng A 810:141035. https://doi.org/10.1016/j.msea.2021.141035
33. Strano G, Hao L, Everson RM, Evans KE (2013) Surface roughness analysis, modelling and prediction in selective laser melting. J Mater Process Technol 213:589–597. https://doi.org/10.1016/j.jmatprotec.2012.11.011
34. Sun Y, Hebert RJ, Aindow M (2018) Non-metallic inclusions in 17–4PH stainless steel parts produced by selective laser melting. Mater Des 140:153–162. https://doi.org/10.1016/j.matdes.2017.11.063
35. Szewczyk NA, Kazior J (2017) Effect of aging temperature on corrosion behavior of sintered 17–4 PH stainless steel in dilute sulfuric acid solution. J Mater Eng Perform 26:3450–3456. https://doi.org/10.1007/s11665-017-2778-4
36. Vilaro T, Colin C, Bartout JD (2011) As-fabricated and heat-treated microstructures of the Ti-6Al-4V alloy processed by selective laser melting. Metall Mater Trans A 42:3190–3199. https://doi.org/10.1007/s11661-011-0731-y
37. Yadollahi A, Shamsaei N, Thompson SM, Elwany A, Bian L (2016) Mechanical and microstructural properties of selective laser melted 17–4 PH stainless steel. Am Soc Mech Eng Digit Collect. https://doi.org/10.1115/IMECE2015-52362
38. Zhao Z, Zhang L, Du W, Bai P, Li J, Zhang W, Yuan X (2022) Microstructure and properties of porous 17–4PH stainless steel prepared by selective laser melting. Trans Indian Inst Met 75:1641–1648. https://doi.org/10.1007/s12666-021-02388-2